electronics

Article

Rapid Extraction of the Fundamental Components for Non-Ideal Three-Phase Grid Based on an Improved Sliding Discrete Fourier Transform

Kai Li and Wei Nai *

Department of Electronic and Information Engineering, Tongji Zhejiang College, Jiaxing 314051, China; likaicumt@163.com
* Correspondence: alexni@tongji.edu.cn; Tel.: +86-189-1852-5982

Abstract: In order to make an effective extraction of the fundamental components for a non-ideal three-phase grid, an improved sliding discrete Fourier transform (ISDFT) has been proposed in this paper. Firstly, the non-ideal signal characteristics are studied in detail, which reveals that there are not only typical harmonic components, but also double frequency components, that exist in dq coordinates when the three-phase grid voltages are unbalanced. Then, the structure form of the conventional sliding discrete Fourier transform (SDFT) has been redesigned to form the ISDFT algorithm, in which a special offset link is introduced to reduce the extraction time while the effectiveness is guaranteed. The experimental results show that this proposed ISDFT is suitable for types of non-ideal signals extraction and can keep a nice dynamical and steady performance in cases of grid or load disturbance. For the average extraction time, ISDFT is saving about 44.56% more of the time than SDFT and about 65.32% more than discrete Fourier transform (DFT).

Keywords: non-ideal three-phase grid; improved sliding discrete Fourier transfer (ISDFT); harmonic components; double frequency components

Citation: Li, K.; Nai, W. Rapid Extraction of the Fundamental Components for Non-Ideal Three-Phase Grid Based on an Improved Sliding Discrete Fourier Transform. *Electronics* **2022**, *11*, 1915. https://doi.org/10.3390/electronics11121915

Academic Editor: Ahmed F. Zobaa

Received: 6 May 2022
Accepted: 17 June 2022
Published: 20 June 2022

1. Introduction

With the popularization of high-power switching equipment in power electric systems and the promotion of large-scale new energy grid connection systems, various non-ideal voltage conditions, including voltage imbalance, harmonic interference, etc., have become a major problem affecting power quality, which would affect the performance of grid-side power instruments, e.g., active power filters, grid-connected converters of renewable and distributed generation systems and so on [1–4]. The fast and accurate estimation of the fundamental components is a key requirement for realizing a reliable operation for these grid-connected instruments [5,6].

Basically, signal extraction methods can be generally categorized into time-domain methods and frequency-domain methods [2,7]. For the time-domain methods, the Taylor–Kalman filter and its improved strategies are the major measures. For example, an extended Taylor–Kalman filter was used for the three-phase system [8], and in [9], an adaptive Kalman filter method was designed for the dynamic estimation of harmonic components. In [10], a filter bank and a self-tuning adaptive filter have been combined for the power signals estimation, in which the filter bank was used to separate odd and even harmonic components while the adaptive filter was used to improve the estimation accuracy. In [11], a modified Taylor–Kalman filter was designed for the dynamic phasor and the time-varying harmonics in a non-steady power system, based on which the total harmonic distortion was reduced. Besides, a rotational invariance technique-based adaptive wavelet neural network (AWNN) was used to improve the power quality [5].

The frequency-domain methods usually refer to Fourier transform-based techniques [12–15], within which the sliding discrete Fourier transform (SDFT) has gained wide applications in recent years for its efficient iteration and easy digital implementation. In [16], the SDFT was used for harmonic detection in the three-phase grid-tie inverter system; besides, SDFT has been often used in cooperation with the phase-locked loop for the stable operation and control of the grid-connected converters [17,18]. Although the SDFT algorithm is computationally efficient, this method still might have drawbacks, e.g., a slow dynamic performance and sensitivity to the frequency, and types of measures have been researched to make improvements [19], and types of improvements have been carried out in [20]. In [21], an adaptive sampling frequency based on the phase error was designed for the SDFT algorithm to improve the estimation accuracy. In [22], a cosine look-up table loop was designed to improve the SDFT-based phase locked loop (PLL) scheme by which the damping factor effect was solved. In [1], a fixed sampling period SDFT and the instantaneous symmetrical components were employed in a pre-loop stage for the pre-filtered synchronous reference frame PLL. For the extreme frequency signals, a new SDFT algorithm was analyzed and designed in [23]; besides, deep comparisons between different frequency-domain methods, such as discrete Fourier transform (DFT), hopping DFT (HDFT), SDFT and modulated HDFT (mHDFT), have been made in [24]. In [5], a generalized discrete Fourier transform (GDFT) was proposed to make further simplifications, which has been realized with great performance and flexibility.

With the consideration that there are not only harmonic components but other unbalanced situations within a non-ideal grid, e.g., amplitude and phase unbalances, and frequency instabilities, in this paper an improved SDFT (ISDFT) strategy has been studied to realize the rapid extraction of fundamental components. The structure of this paper is as follows. The characteristics of the non-ideal three-phase grid are analyzed in detail in Section 2. This new ISDFT strategy is designed in Section 3, including a theoretical comparison with the normal SDFT strategy. Section 4 contains the results analysis and comparison, while the conclusion and outlook are given in Section 5.

2. Characteristics of the Non-Ideal Grid

For a typical three-phase three-wire voltage-sourced converter, when the grid is unbalanced, the grid-side voltage $\boldsymbol{e}$ can be decomposed into the positive sequence $\boldsymbol{e}^{\mathrm{P}}$ and negative sequence $\boldsymbol{e}^{\mathrm{N}}$.

Firstly, assuming only the fundamental components are being considered and ignoring the saturation effect of the line impedance on the grid-side, according to the basic expression of the non-ideal grid system, the grid-side voltage $\boldsymbol{e}$ can be expressed as Equation (1) in ABC stationary coordinates:

$$\begin{bmatrix} e_{\mathrm{a}} \\ e_{\mathrm{b}} \\ e_{\mathrm{c}} \end{bmatrix} = E_{\mathrm{m}}^{\mathrm{P}} \begin{bmatrix} \cos(\omega t + \alpha_{\mathrm{P}}) \\ \cos(\omega t + \alpha_{\mathrm{P}} - 120^\circ) \\ \cos(\omega t + \alpha_{\mathrm{P}} + 120^\circ) \end{bmatrix} + E_{\mathrm{m}}^{\mathrm{N}} \begin{bmatrix} \cos(\omega t + \alpha_{\mathrm{N}}) \\ \cos(\omega t + \alpha_{\mathrm{N}} - 120^\circ) \\ \cos(\omega t + \alpha_{\mathrm{N}} + 120^\circ) \end{bmatrix}, \quad (1)$$

where e_{a}, e_{b} and e_{c} are grid-side voltage components in ABC stationary coordinates, and $E_{\mathrm{m}}^{\mathrm{P}}$, $E_{\mathrm{m}}^{\mathrm{N}}$ are the corresponding voltage amplitudes, respectively; ω is the grid angular frequency, and α_{P} and α_{N} are the initial phase angles of the positive and negative sequences, respectively.

Taking ω as the rotational angular frequency, Equation (1) can be transformed as Equation (2) in the rotational coordinates (dq coordinates):

$$\begin{bmatrix} e_{\mathrm{d}} \\ e_{\mathrm{q}} \end{bmatrix} = \sqrt{\frac{3}{2}} E_{\mathrm{m}}^{\mathrm{P}} \begin{bmatrix} \cos(\alpha_{\mathrm{P}}) \\ \sin(\alpha_{\mathrm{P}}) \end{bmatrix} + \sqrt{\frac{3}{2}} E_{\mathrm{m}}^{\mathrm{N}} \begin{bmatrix} \cos(2\omega t + \alpha_{\mathrm{N}}) \\ -\sin(2\omega t + \alpha_{\mathrm{N}}) \end{bmatrix}. \quad (2)$$

It is obvious that when the grid voltage is unbalanced, there are double frequency components ($2\omega t$) existing in the dq coordinates, even when only fundamental components are being considered. However, the unbalanced grid usually contains typical harmonic components, e.g., ($6k \pm 1$)-th (k = 1, 2, 3 ...) harmonics. For example, when a 20% amplitude is falling within the A-phase at t = 0.05 s, the double frequency component existing in the d coordinates is shown in Figure 1.

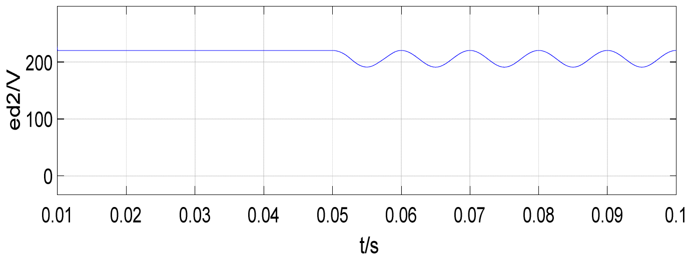

Figure 1. Double frequency component in d coordinates with amplitude unbalance.

To make an effective information extraction of the unbalanced grid, an improved SDFT method is proposed in this paper to extract both the typical harmonic components in ABC stationary coordinates and double frequency components in the dq coordinates. The block diagram of the proposed extraction method is shown in Figure 2 (Here, the signal sampling frequency is assumed to be much higher than the frequency of the grid-side voltages including both the fundamental and typical harmonic components), where $\boldsymbol{e}_{\mathrm{abc}}$ are the original unbalanced grid voltages in the ABC coordinate, $\boldsymbol{e}^{\mathrm{h}}_{\mathrm{abc}}$ represent the extracted typical harmonic components, $\boldsymbol{e}_{\mathrm{dq}}$ are the unbalanced grid voltages in the dq coordinate, $\boldsymbol{e}^{2}_{\mathrm{dq}}$ are the extracted double frequency components, and $\boldsymbol{e}^{*}_{\mathrm{dq}}$ represent the ideal grid voltages in the dq coordinate, while $\boldsymbol{e}^{*}_{\mathrm{abc}}$ are the output grid voltages in the ABC coordinate.

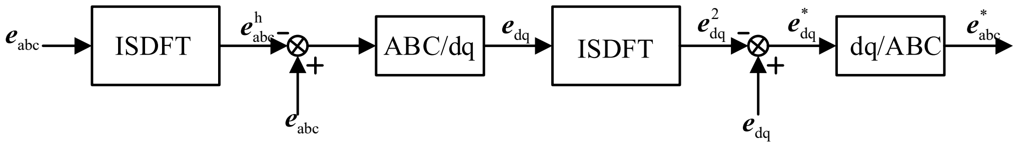

Figure 2. Block diagram of the proposed method based on ISDFT.

3. Signals Extraction

3.1. Traditional SDFT

Usually, the non-ideal grid voltage could be taken as a finite data sequence $v(m)$ whose length is M; its DFT can be written as:

$$V(k) = DFT[v(m)] = \sum_{n=0}^{M-1} v(k)W_M^{nk}, (0 \le k \le M-1), \tag{3}$$

where $W_M = e^{-j2\pi/M}$.

Obviously, Equation (3) can be extended as:

$$V(k) = v(0) + v(1)e^{-j\frac{2\pi k}{M}} + v(2)e^{-j\frac{2\pi k\times 2}{M}} + \ldots + v(M-1)e^{-j\frac{2\pi k\times(M-1)}{M}}. \tag{4}$$

Defining the first sampling sequence of data, $v(m)$ is $v(0)$, the corresponding discrete data are from $v(0)$ to $v(M-1)$, and the DFT of sequence v_0 is $V_0(k)$; the second sampling sequence is $v(1)$, the corresponding data are from $v(1)$ to $v(M)$, and the DFT is $V_1(k)$.

On the basis of Equation (4), the following relationship exists between $V_0(k)$ and $V_1(k)$:

$$V_1(k) = [V_0(k) - v(0)]e^{j\frac{2\pi k}{M}} + v(M)e^{-j\frac{2\pi k\times(M-1)}{M}} = [V_0(k) - v(0) + v(M)]e^{j\frac{2\pi k}{M}}. \tag{5}$$

Equation (5) is the traditional and universal SDFT algorithm, which is suitable for the digital implementation because of the lesser computational effort, and the different k value means a different harmonic order.

According to Equation (5), the SDFT of the m-th sequence is:

$$V_{\mathrm{m}}(k) = [V_{\mathrm{m-1}}(k) - v(m-1) + v(m+M-1)]e^{j\frac{2\pi k}{M}}, \tag{6}$$

where $V_{\mathrm{m}}(k)$ is the DFT of the m-th sequence, the corresponding data are from $v(m)$ to $v(m + M - 1)$, while $V_{\mathrm{m}-1}(k)$ is the DFT of the previous $(m - 1)$-th sequence, whose discrete data are from $v(m - 1)$ to $v(m + M - 2)$.

In the time domain, the k-th harmonic of the m-th sequence can be written as:

$$V^k(m) = \frac{1}{M} V_{\mathrm{m}}(k) e^{j2\pi \frac{km}{M}}. \tag{7}$$

In this paper, the m-th sequence is taken as the input non-ideal grid signal, and the extracted k-th harmonic component is the output signal, so the transfer function in the z-domain could be settled as:

$$G^k(z) = \frac{Z\left[\frac{1}{M} V_{\mathrm{m}}(k) e^{j2\pi \frac{km}{M}}\right]}{Z[v(k)]} = \underbrace{(1 - z^{-M})}_{H_c(z)} \underbrace{\left(\frac{1}{1 - z^{-1} e^{j2\pi \frac{k}{M}}}\right)}_{H_r^k(z)} \underbrace{\frac{1}{M} e^{j2\pi \frac{k}{M}}}_{\lambda}. \tag{8}$$

In Equation (8), the first part $H_{\mathrm{c}}(z)$ is an important link, and it could be extended as:

$$H_{\mathrm{c}}(z) = 1 - z^{-M} = \prod_{n=0}^{M-1} (1 - e^{j2\pi \frac{n}{M}} z^{-1}). \tag{9}$$

Equation (9 introduces M zeros centered on $\omega = \lambda\omega_0$, where $\omega_0 = 2\pi/M$, $\lambda = 0, 1, \ldots, M - 1$; all the zeros are distributed on a unit circle, and each zero means one frequency harmonic that could be eliminated by a proper setting.

In Equation (8), the second part $H_{\mathrm{r}}{}^k(z)$ produces a pole; when $\omega = k\omega_0$, the pole and one zero cancel each other, and then the k-th harmonic component could be extracted; the corresponding diagram of pole-zero cancellation is shown in Figure 3 (M = 24 and k = 5). The third part λ in Equation (8) plays the role of adjusting the amplitude of the extracted k-th harmonic, and the structure diagram of this traditional SDFT is shown in Figure 4.

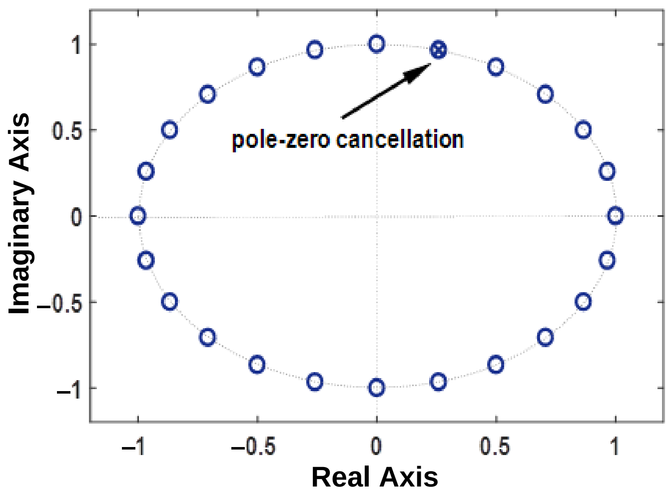

Figure 3. Pole-zero diagram of SDFT (M = 24 and k = 5).

Obviously, for the traditional SDFT, the $H_{\mathrm{c}}(z)$ part determines the harmonic components that could be extracted, which here means all the integer harmonic components, for $\omega = \lambda\omega_0$ ($\lambda = 0, 1, \ldots, M{-}1$). However, more zeros mean more delay links (M zeros mean M delay links), and in some cases, for not all the zeros, the results are required in an unnecessary time delay.

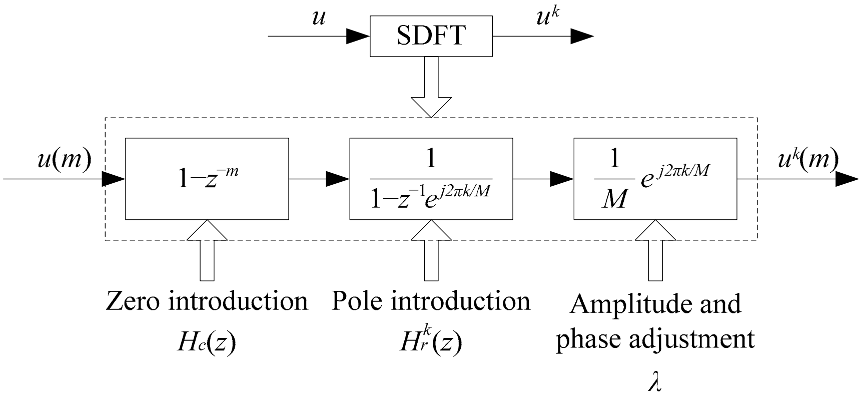

Figure 4. Structure diagram of the SDFT algorithm.

3.2. Proposed ISDFT

When considering the characteristics of the researched non-ideal grid system, the improved SDFT is studied by redesigning H_c(z). According to the transfer function of traditional H_c(z) shown in Equation (9), it is explained that M zeros are introduced at the integral multiple fundamental frequency, which can be expressed as $\omega = \lambda\omega_0$ (λ = 0, 1, ..., $M - 1$); these zeros are uniformly distributed on the unit circle to realize the complete elimination of corresponding frequency harmonics. However, the actual system does not necessarily contain all the harmonics corresponding to all of the above zero points. In addition, if all the harmonics are eliminated, this will also cause a time delay. According to the characteristic analysis of the non-ideal power grid, the main harmonic order in the power grid voltage is $k = 6h \pm 1$ (h = 1, 2, 3, ...) and k = 2. Therefore, $z = z^{1/6}e^{-j2\pi/6M}$, $z = z^{1/6}e^{j2\pi/6M}$, and $z = z^{1/2}$ are substituted into Equation (9), respectively, and thus H_c(z) can be redesigned as:

$$H_{c1}(z) = (1 - z^{-\frac{M}{6}} e^{-j\frac{2\pi}{6}})(1 - z^{-\frac{M}{6}} e^{-j\frac{2\pi}{6}}) = \prod_{n=0}^{N-1}(1 - e^{j2\pi\frac{6k+1}{6M}} z^{-\frac{1}{6}}) \prod_{n=0}^{N-1}(1 - e^{j2\pi\frac{6k+1}{6M}} z^{-\frac{1}{6}}), \tag{10}$$

$$H_{c2}(z) = 1 - z^{-\frac{M}{2}}. \tag{11}$$

Then, the transfer function of ISDFT can be rewritten as:

$$G_{6h+1}^k(z) = \underbrace{(1 - z^{-\frac{M}{6}} e^{-j\frac{2\pi}{6}})(1 - z^{-\frac{M}{6}} e^{-j\frac{2\pi}{6}})}_{H_{c1}(z)} \underbrace{\left(\frac{1}{1 - z^{-1}e^{j2\pi\frac{k}{M}}}\right)}_{H_\tau^k(z)} \underbrace{\frac{1}{M}e^{j2\pi\frac{k}{M}}}_{\lambda}, \tag{12}$$

$$G_{2h}^k(z) = \underbrace{(1 - z^{-\frac{M}{2}})}_{H_{c2}(z)} \underbrace{\left(\frac{1}{1 - z^{-1}e^{j2\pi\frac{k}{M}}}\right)}_{H_\tau^k(z)} \underbrace{\frac{1}{M}e^{j2\pi\frac{k}{M}}}_{\lambda}. \tag{13}$$

The corresponding structure diagrams are shown in Figure 5a,b.

Now, the zeros of the ISDFT algorithm become $\omega = (6h \pm 1)\omega_0$ and $\omega = 2\omega_0$, and the number of system zero points becomes $M/6 + M/6 = M/3$ and $M/2$, respectively. Compared with SDFT, the numbers of zeros are one third of that and half of the original, which means that the delay times of ISDFT are also reduced to one third and half of the SDFT. The corresponding pole-zero diagrams when M = 24 and k = 5, M = 24 and k = 2 are shown in Figure 6a,b.

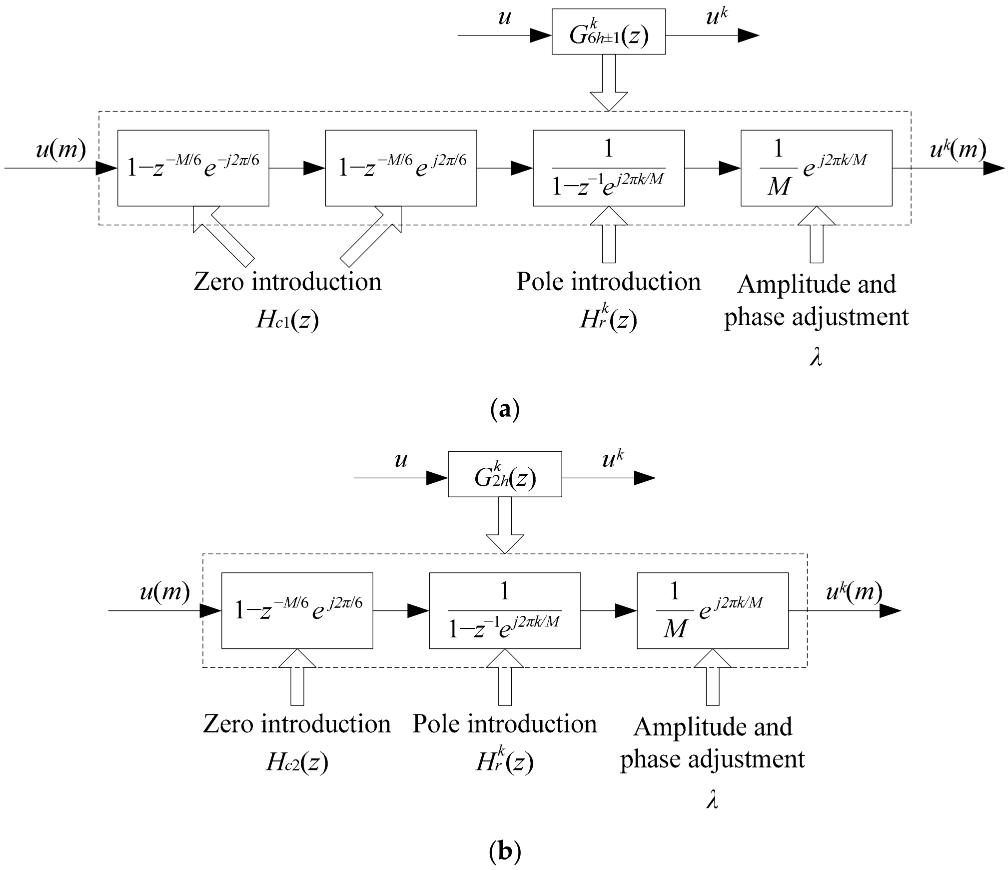

Figure 5. Structure diagram of the ISDFT algorithm: (**a**) $G^k_{6h+1}(z)$; (**b**) $G^k_{2h}(z)$.

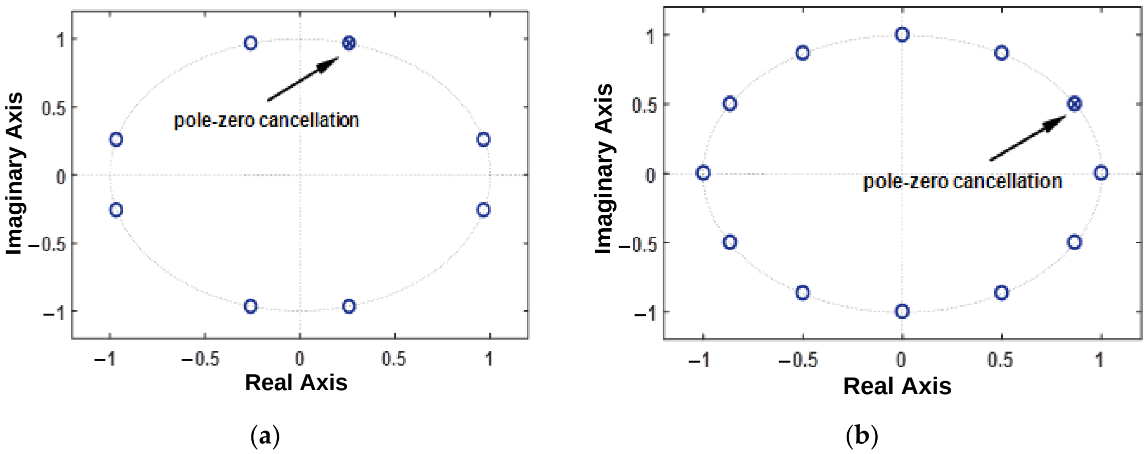

Figure 6. Pole-zero diagrams of this ISDFT algorithm: (**a**) Pole-zero diagram of the ISDFT algorithm (M = 24, k = 5); (**b**) Pole-zero diagram of the ISDFT algorithm (M = 24, k = 2).

According to above analysis, the extraction flow chart of the fundamental components for the non-ideal three-phase grid is shown in Figure 7.

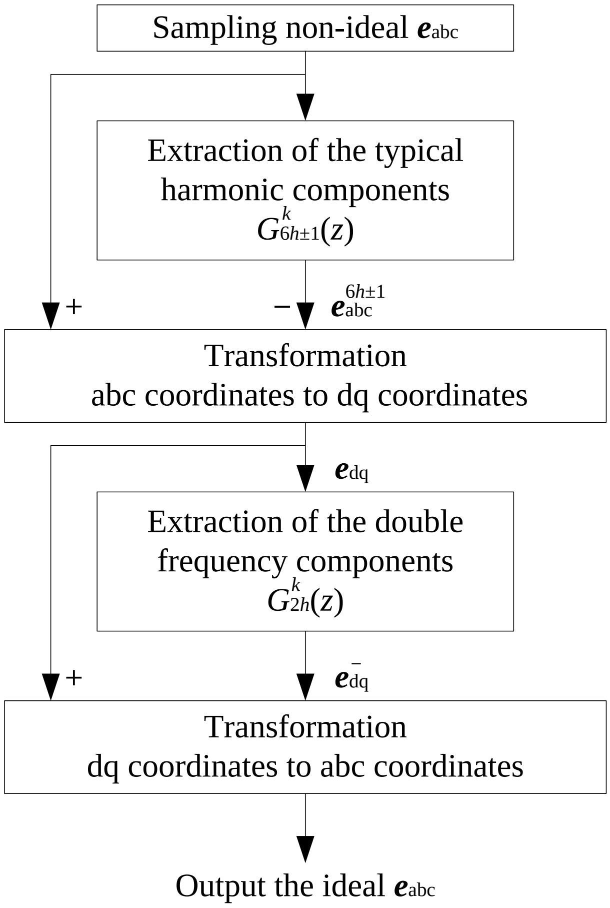

Figure 7. Extraction flow chart of the fundamental components.

4. Experimental Results

The established platform used for the experimental verification is displayed in Figure 8, including a programmable three-phase AC source which could simulate various non-ideal grids, a signal processing system based on TMS320F28335 DSP to deal with the ISDFT algorithm studied in this paper, and an oscilloscope to display the execution results.

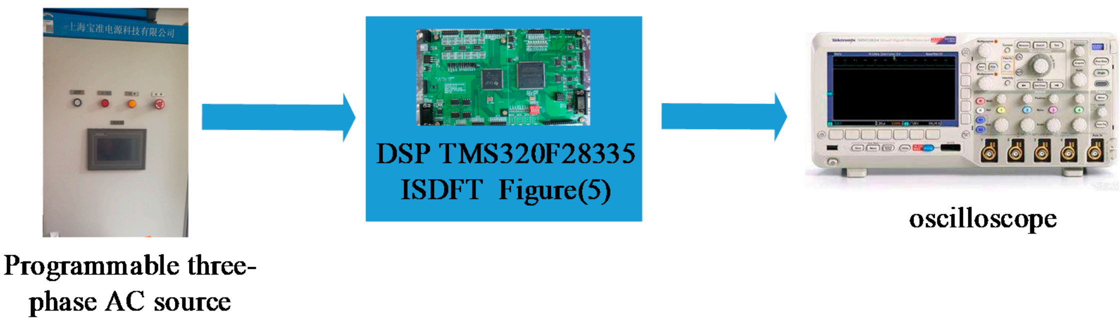

Figure 8. Experimental platform.

4.1. Signal Tracking Performance

With a static input signal $u_{in} = \sin(500\pi t)$, the tracking waveforms by ISDFT, DFT and SDFT are compared in Figure 9.

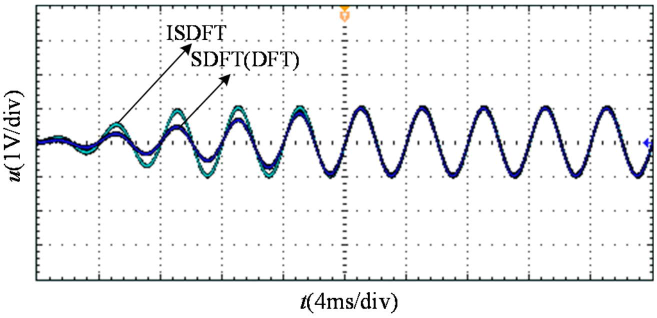

Figure 9. Tracking waveforms with a static input.

Obviously, the tracking time of ISDFT is about two cycles, while it is about five cycles for SDFT and DFT. When t = 0.2 s, the input amplitude is doubled (1 V → 2 V), and the dynamic tracking results are shown in Figure 10.

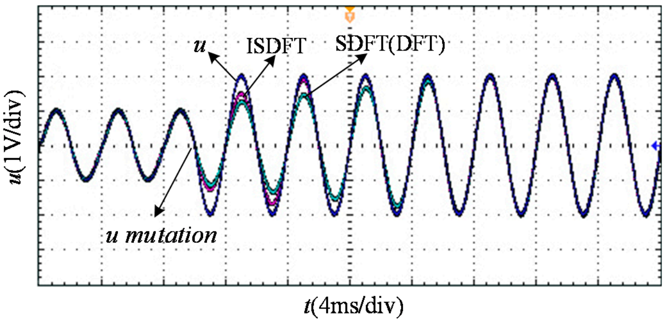

Figure 10. Dynamic voltage waveforms.

Similarly, for ISDFT, the dynamic response time is about two cycles, while it is about five cycles for SDFT. From the above experimental waveforms, it can be seen that the signal tracking performance of DFT, SDFT and ISDFT is the same.

4.2. Harmonic Extraction

For the harmonic extraction, e.g., when there are 5th and 7th harmonic components existing in the A-phase and B-phase, as shown in Figure 11a,b, the extracted harmonic components with ISDFT are shown in Figure 11c,d, and the three-phase waveforms after the harmonics elimination are shown in Figure 11e,f. Note that the scales are changed in inlets in Figure 11a,c,d and e.

The series experimental results shown in Figures 10 and 11 can validate the effectiveness of the studied ISDFT algorithm; the dynamic response time is about half of one cycle (10 ms).

For the ISDFT, SDFT and DFT algorithms, the execution times of the extraction of the 5th and 7th harmonic components are compared in Table 1.

Table 1. Comparison of the harmonic extraction time.

Harmonic Extraction Method	5th Harmonic Extraction Time (μs)	7th Harmonic Extraction Time (μs)
DFT	251.41	228.93
SDFT	157.28	143.22
ISDFT	87.19	78.62

The ISDFT is approximately saving about 44.56% more of the time than the SDFT, and about 65.32% more of the time than the DFT.

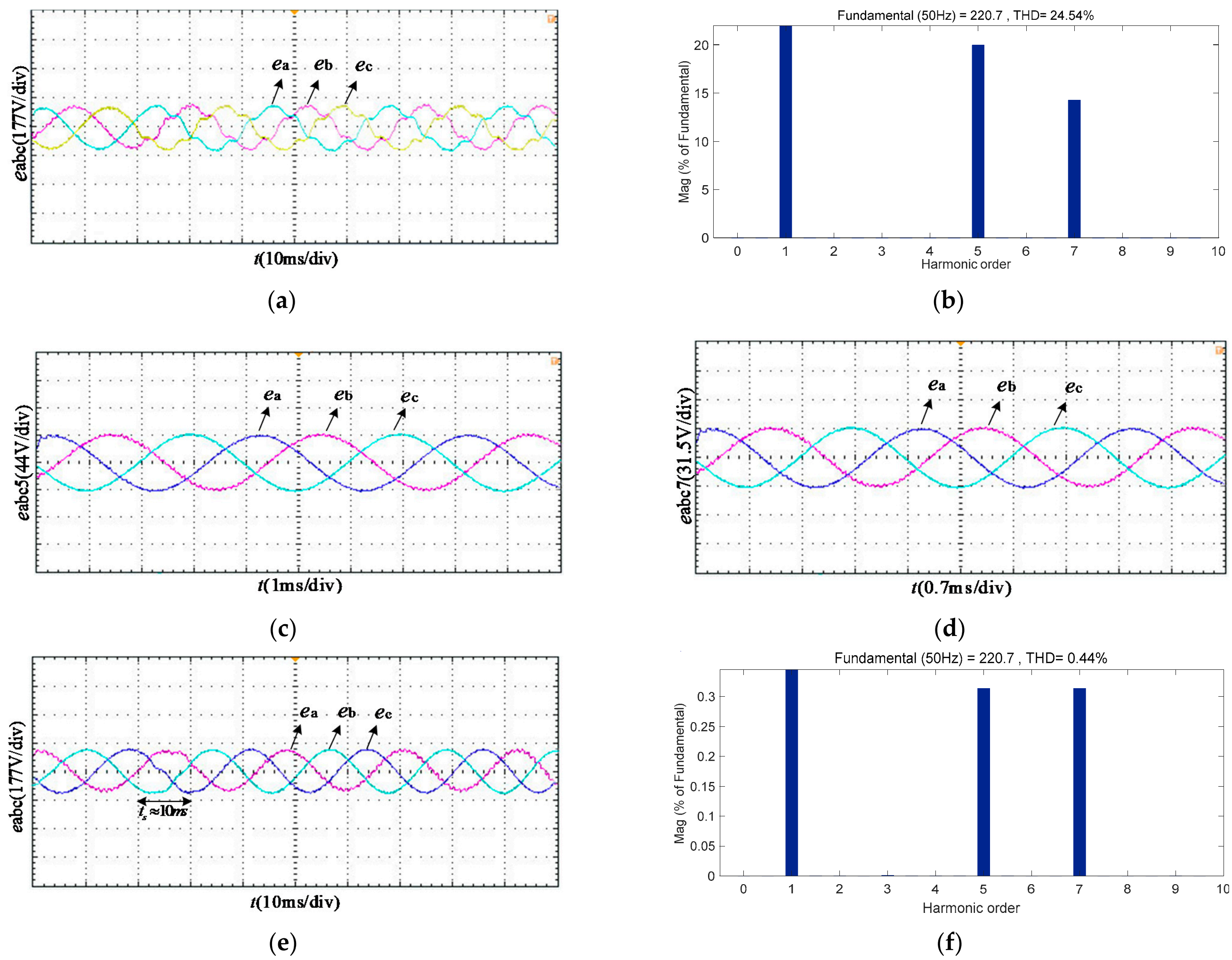

Figure 11. Harmonics extraction based on ISDFT algorithm: (**a**) Non-ideal three-phase voltages with harmonic components; (**b**) FFT analysis of the non-ideal three-phase voltages (5th: 19.97%; 7th: 14.27%); (**c**) Extracted 5th harmonic component; (**d**) Extracted 7th harmonic component; (**e**) Three-phase voltages after harmonics elimination; (**f**) FFT analysis of three-phase voltages after harmonics elimination (5th: 0.31%; 7th: 0.31%).

4.3. Other Non-Ideal Signals Extraction

When there is a sudden 20% amplitude disturbance within the A-phase voltage at t = 10 ms and t = 50 ms, as shown in Figure 12a, the extracted double frequency components (e_d^2 and e_q^2) in the dq coordinates are shown in Figure 12b,c, and the three-phase voltages after the non-ideal components elimination are shown in Figure 12d. Note that the scales are changed in inlets Figure 12a–d.

Similarly, when there is a sudden 12° phase disturbance within the A-phase voltage at t = 20 ms, as shown in Figure 13a, the extracted double frequency components (e_d^2 and e_q^2) in the dq coordinates are shown in Figure 13b,c, and the three-phase voltages after the non-ideal components elimination are shown in Figure 13d. Note that the scales are changed in inlets in Figure 13a–d.

When there is a sudden 0.5 Hz frequency disturbance within the A-phase voltage at t = 20 ms, as shown in Figure 14a, the extracted double frequency components (e_d^2 and e_q^2) in the dq coordinates are shown in Figure 14b,c, and the three-phase voltages after the non-ideal components elimination are shown in Figure 14d. Note that the scales are changed in inlets in Figure 14a–d.

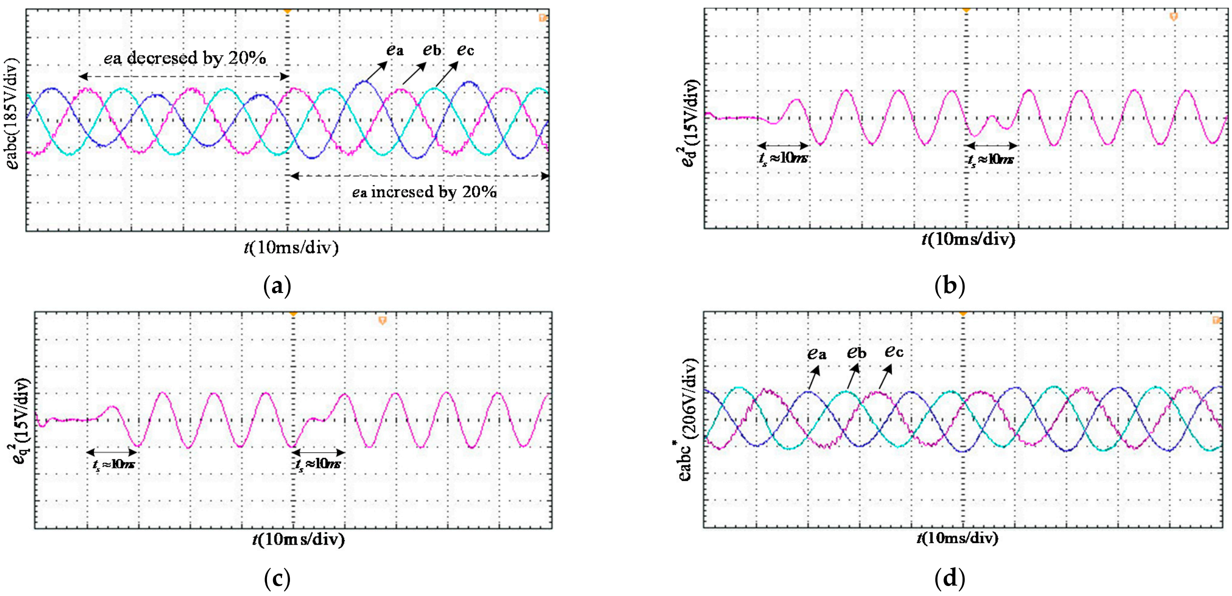

Figure 12. Non-ideal signals extraction based on ISDFT algorithm (Amplitude disturbance): (**a**) The non-ideal grid voltages with amplitude disturbance in A-phase; (**b**) The extracted double frequency component in d-axis; (**c**) The extracted double frequency component in q-axis; (**d**) Three-phase voltages after non-ideal components elimination.

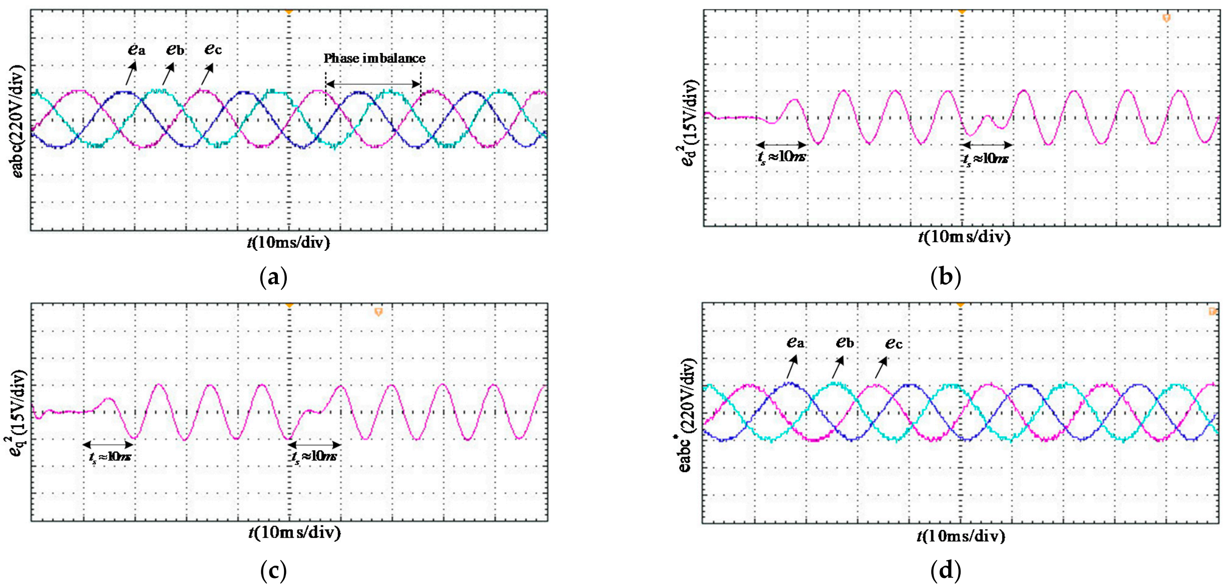

Figure 13. Non-ideal signals extraction based on ISDFT algorithm (Phase disturbance): (**a**) The non-ideal grid voltages with phase disturbance in A-phase; (**b**) The extracted double frequency component in d-axis; (**c**) The extracted double frequency component in q-axis; (**d**) Three-phase voltages after non-ideal components elimination.

4.4. Non-Ideal Signals Extraction Considering Load Changes

When taking the amplitude modulation as an example and under an amplitude of phase a reduced by 20%, at t = 20 ms, the three-phase load is suddenly changed, as shown in Figure 15a, the extracted double frequency components (e_d^2 and e_q^2) in the dq coordinates are shown in Figure 15b,c, and the three-phase voltages after the non-ideal components elimination in the dq coordinates are shown in Figure 15d,e, while the corresponding three-phase voltages after the non-ideal components elimination in the ABC coordinates are shown in Figure 15f. Note that the scales are changed in inlets in Figure 15a–f.

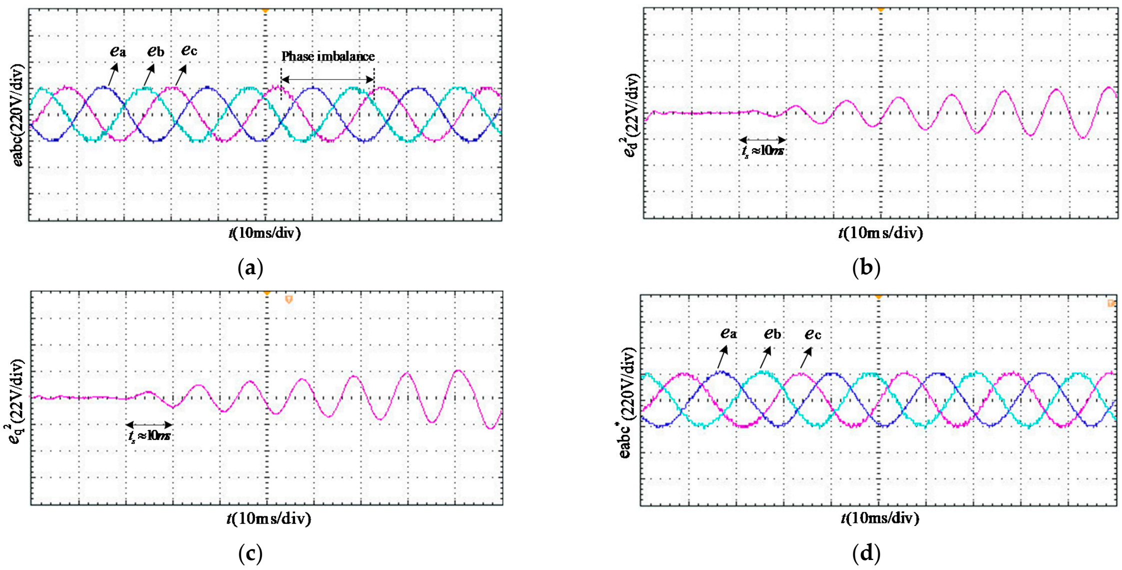

Figure 14. Non-ideal signals extraction based on ISDFT algorithm (Frequency disturbance): (**a**) The non-ideal grid voltages with frequency disturbance in A-phase; (**b**) The extracted double frequency component in d-axis; (**c**) The extracted double frequency component in q-axis; (**d**) Three-phase voltages after non-ideal components elimination.

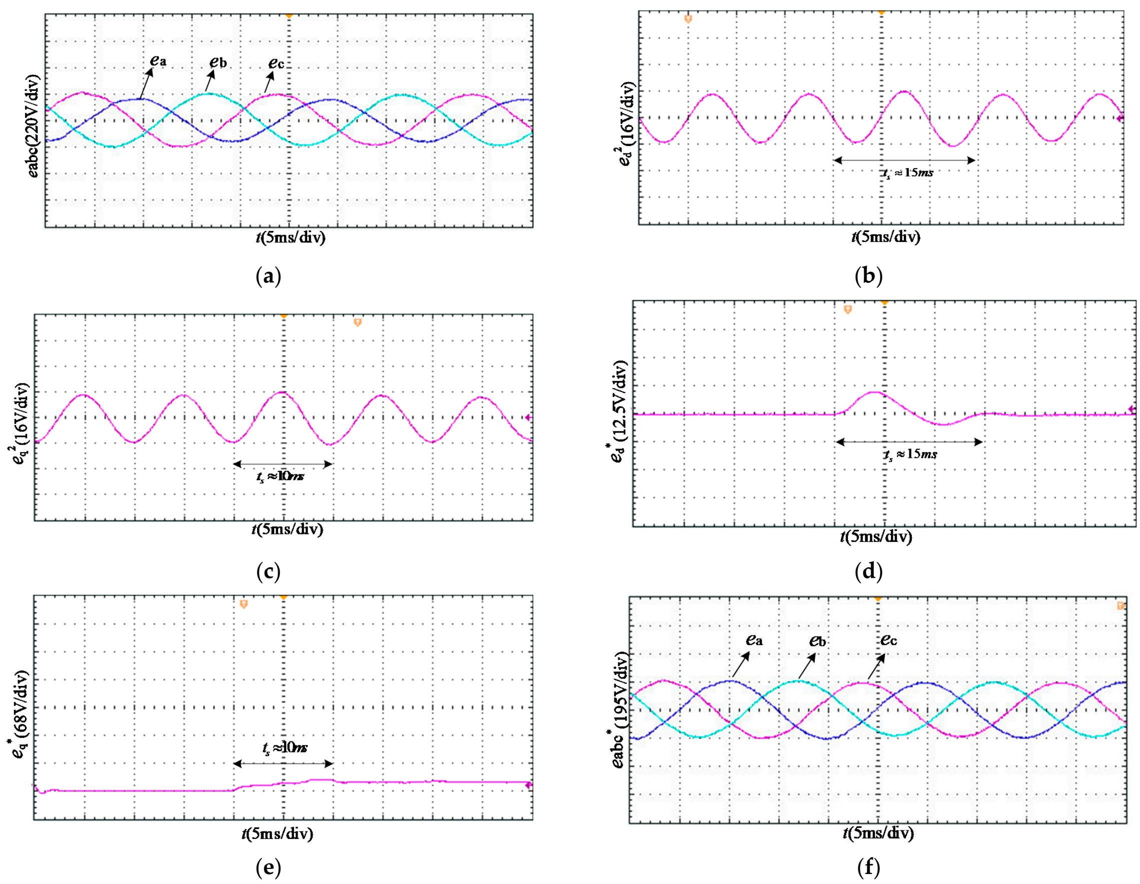

Figure 15. Non-ideal signals extraction considering load change based on ISDFT algorithm (Amplitude disturbance): (**a**) The non-ideal grid voltages with the three-phase load suddenly changed; (**b**) The extracted double frequency component in d-axis; (**c**) The extracted double frequency component in q-axis; (**d**) Voltage in d-axis after non-ideal components elimination; (**e**) Voltage in q-axis after non-ideal components elimination; (**f**) Three-phase voltages after non-ideal components elimination.

This ISDFT algorithm could also work with a dynamic change of load, and the average response time is less than one cycle (20 ms), which verifies the validity and applicability of this improved algorithm.

5. Conclusions

In this paper, an improved sliding discrete Fourier Transform (ISDFT) has been studied for the signal extraction of a non-ideal three-phase grid. Besides there being harmonic components in the three-phase voltages, there would be double frequency components existing in the dq coordinates when the three-phase voltages are unbalanced. With the redesigning of the transforms of the normal sliding discrete Fourier transform (SDFT), the typical harmonic components and double frequency components could be respectively extracted, along with less extraction time, while the effectiveness was guaranteed.

Different types of experiments, including signal tracking performance, harmonic extraction, and signals extraction with different non-ideal cases, were carried out, which verified that this studied ISDFT algorithm is suitable for types of non-ideal signals extraction with a nice dynamical and steady performance, and the average extraction time was much lower than for the normal DFT or SDFT algorithm, which makes it easier to use in digital implementations.

As the proposed ISDFT algorithm has a strong signal extraction ability in terms of dealing with a non-ideal power grid or load disturbance, in the future, from a macro perspective, one could consider applying it to the analysis of large-scale new energy grid connections in the background of non-ideal power grids; additionally, from a micro perspective, one could also consider applying it to the analysis of unstable signals in synchrophasors.

Author Contributions: Conceptualization, K.L.; methodology, K.L. and W.N.; validation, K.L. and W.N.; formal analysis, K.L. and W.N.; writing—original draft preparation, K.L.; writing—review and editing, W.N.; funding acquisition, W.N. All authors have read and agreed to the published version of the manuscript.

Funding: This work was supported in part by the Science and Technology Commission of Shanghai Foundation under Grant No. 19DZ1205804, the Jiaxing Public Welfare Research Project under Grant No. 2020AY10033, No. 2020AY30025, and No. 2021AY10079, and the General Scientific Research Fund of Zhejiang Provincial Education Department under Grant No. Y202147878.

Data Availability Statement: The processed data required to reproduce these findings cannot be shared at this time as the data also forms part of an ongoing study.

Conflicts of Interest: The authors declare no conflict of interest.

References

1. Subramanian, C.; Kanagaraj, R. Rapid tracking of grid variables using prefiltered synchronous reference frame PLL. *IEEE Trans. Instrum. Meas.* **2015**, *64*, 1826–1836. [CrossRef]
2. Asiminoaei, L.; Blaabjerg, F.; Hansen, S. Detection is key—Harmonic detection methods for active power filter applications. *IEEE Ind. Appl. Mag.* **2007**, *13*, 22–33. [CrossRef]
3. Li, Y.W.; He, J. Distribution system harmonic compensation method: An overview of DG-interfacing inverters. *IEEE Ind. Electron. Mag.* **2014**, *8*, 18–31. [CrossRef]
4. Peng, C.; Hu, S.L.; Hao, X.H. An improved detection algorithm of three-phase unbalanced voltage sag detection method for improving power supply reliability. In Proceedings of the 10th International Conference on Quality, Reliability, Risk, Maintenance, and Safety Engineering (QR2MSE), Xi'an, China, 8–11 October 2020. [CrossRef]
5. Jain, S.K.; Singh, S.N. Fast harmonic estimation of stationary and time-varying signals using EA-AWNN. *IEEE Trans. Instrum. Meas.* **2013**, *62*, 335–343. [CrossRef]
6. Yan, H.; Wang, X.; Rui, S. Non-Ideal Power Grid Multi-Target Current Reference Instruction Calculating Method, Involves Suppressing Active Power Pulsation and Current Reference Instruction under Three Control Targets of Power Pulsation Based on Instantaneous Theory. China Patent No. CN110676878-A, 10 January 2020.
7. Liu, H.; Hu, H.; Chen, H.; Zhang, L.; Xing, Y. Fast and flexible selective harmonic extraction methods based on generalized discrete Fourier Transform. *IEEE Trans. Power Electron.* **2018**, *33*, 3484–3496. [CrossRef]

8. Ferrero, R.; Pegoraro, P.A.; Toscani, S. Three-phase synchrophasor estimation through Taylor extended Kalman filtering. In Proceedings of the 10th IEEE International Workshop on Applied Measurements for Power Systems (AMPS), Aachen, Germany, 25–27 September 2019. [CrossRef]
9. Yu, K.K.C.; Watson, N.R.; Arrillaga, J. An adaptive Kalman filter for dynamic harmonic state estimation and harmonic injection tracking. *IEEE Trans. Power Deliv.* **2005**, *20*, 1577–1584. [CrossRef]
10. Sohn, S.-W.; Lim, Y.-B.; Yun, J.-J.; Choi, H.; Bae, H.-D. A filter bank and a self-tuning adaptive filter for the harmonic and interharmonic estimation in power signals. *IEEE Trans. Instrum. Meas.* **2012**, *61*, 64–73. [CrossRef]
11. Maldonado, J.R. Total harmonic distortion estimation, minimization inter harmonic amplitude and expanding bands rejection in TKF filters. *IEEE Lat. Am. Trans.* **2016**, *14*, 652–656. [CrossRef]
12. Jacobsen, E.; Lyons, R. The sliding DFT. *IEEE Signal Processing Mag.* **2003**, *20*, 74–80. [CrossRef]
13. Jacobsen, E.; Lyons, R. An update to sliding DFT. *IEEE Signal Process. Mag.* **2004**, *21*, 110–111. [CrossRef]
14. Sumathi, P. A frequency demodulation technique based on sliding DFT phase locking scheme for large variation FM signals. *IEEE Commun. Lett.* **2012**, *16*, 1864–1867. [CrossRef]
15. Li, K.; Zheng, W.; Li, K. A fast algorithm with less Operations for length-$N = q \times 2^m$ DFTs. *IEEE Trans. Signal Process.* **2015**, *63*, 673–683. [CrossRef]
16. Chen, D. An improved harmonics detection method based on sliding discrete Fourier transform for three-phase grid-tie inverter system. *IEICE Electron. Express* **2019**, *16*, 20181074. [CrossRef]
17. Tan, G.; Fu, Q.; Xia, T.; Zhang, X. Development of frequency fixed sliding discrete Fourier transform filter based single-phase phase-locked loop. *IEEE Access* **2021**, *9*, 110573–110581. [CrossRef]
18. Xu, M.; Sang, Z.; Li, X.; You, Y.; Dai, D. An observer-based harmonic extraction method with front SOGI. *Machines* **2022**, *10*, 95. [CrossRef]
19. Reza, M.S.; Sadeque, F.; Hossain, M.M.; Ghias, A.M.Y.M.; Agelidis, V.G. Three-phase PLL for grid-connected power converters under both amplitude and phase unbalanced conditions. *IEEE Trans. Ind. Electron.* **2019**, *66*, 8881–8891. [CrossRef]
20. Lyons, R.; Howard, C. Improvements to the sliding discrete Fourier transform algorithm. *IEEE Signal Process. Mag.* **2021**, *38*, 119–127. [CrossRef]
21. Sumathi, P.; Janakiraman, P.A. Integrated phase-locking scheme for SDFT-based harmonic analysis of periodic signals. *IEEE Trans. Circuits Syst. II Express Briefs* **2008**, *55*, 51–55. [CrossRef]
22. Sumathi, P.; Janakiraman, P.A. Phase locking scheme based on look-up-table-assisted sliding discrete Fourier transform for low-frequency power and acoustic signals. *IET Circuits Devices Syst.* **2011**, *5*, 494–504. [CrossRef]
23. Shen, T.; Chen, L.; Guan, J.; Duan, J. A new sliding frequency Fourier transform phase difference measurement method for extreme frequency signals. *Rev. Sci. Instrum.* **2020**, *91*, 015103. [CrossRef]
24. Tyagi, T.; Sumathi, P. Comprehensive performance evaluation of computationally efficient discrete Fourier transforms for frequency estimation. *IEEE Trans. Instrum. Meas.* **2019**, *69*, 2155–2163. [CrossRef]